Korean J. Chem. Eng., 40(5), 1055-1062 (2023)
DOI: 10.1007/s11814-023-1435-x

pISSN: 0256-1115
eISSN: 1975-7220

Enhanced catalytic complete oxidation of 1,2-dichloroethane to CO_2 over the Al-based oxide supported $CuCl_x$ composite catalysts

Seungjun Lee, Wongeun Yoon, Iljun Chung, Junil Choi, Yongju Yun, and Won Bae Kim†

Department of Chemical Engineering, Pohang University of Science and Technology (POSTECH), 77 Cheongam-ro, Nam-gu, Pohang, Gyeongbuk 37673, Korea
(*Received 27 October 2022 • Revised 21 December 2022 • Accepted 31 January 2023*)

Abstract−Chlorinated volatile organic compounds (CVOCs) have been regarded as hazardous atmospheric pollutants, and catalytic oxidative destruction has been considered as the most efficient method to handle such contaminants. Herein, characteristics of Al, Si and Ti based supporting materials were modified with cupric chloride to enhance catalytic performance for the complete oxidation of 1,2-dichlroethane (DCE). According to the supporting materials in the presence or absence of active materials, physicochemical properties of catalysts appear to be quite differentiated, and the relationship between modified properties and its catalytic performance was observed and discussed. Among the studied catalysts, $CuCl_2/Al_1Ti_1O_x$ composite showed the highest catalytic performance, which could be attributed to several beneficial effects associated with proper textural property, abundant acid sites and oxidizing ability. This catalyst designing strategy described in this study suggests a prospective way to develop efficient catalysts fashioned of non-precious, earth-abundant materials for the catalytic oxidation of CVOCs.

Keywords: Chlorinated VOCs (CVOCs), Catalytic Complete Oxidation, Composite Catalytic Material, Dehydrochlorination, Surface Modification

INTRODUCTION

The emission of artificial hazardous pollutants has increased rapidly. Among them, volatile organic compounds (VOCs) are discharged regardless of the scope of human activity (such as home life, industry and transportation), which can significantly affect the environment while circulating in the atmosphere [1]. Recently, various methods have been newly attempted [2-4], but traditional catalytic oxidation is still considered one of the most effective removal methods for VOCs because of low operating temperatures and products formation of non-toxic H_2O and CO_2 [5]. However, some VOCs containing Cl element would make its catalytic removal process to be even more difficult [6]. When these chlorinated VOCs (CVOCs) are not completely oxidized, polychlorinated byproducts (which are frequently much toxic than the original CVOCs) could be emitted. Moreover, the Cl-species can function as poisoning agents, causing deactivation by covering the surface of catalyst where the reactant molecules could be adsorbed and converted. Thus, in order to properly remove CVOCs, the catalyst should not only be active, but also be chemically stable under Cl-containing atmosphere with high selectivity toward non-toxic products.

It has been reported that the mechanism of catalytic destruction of CVOCs could be quite different depending on physicochemical properties of catalyst [7]. Among the reported mechanisms, it is widely accepted that the CVOCs could be removed much readily when the C-Cl bonds were cleaved first and the residual intermediates were decomposed after [7-12]. For the C-Cl bond cleavage as an initiation step, acid sites of the surface of catalyst play an important role and HCl molecules are released (i.e., dehydrochlorination) from the original CVOCs. Afterward, dehydrochlorinated intermediate is further oxidized by the oxygen species present on surface of the catalysts, and it is a much easier route compared with the direct destruction of original CVOCs. In this sense, it could be deduced that the catalyst should possess both of proper acidic properties and excellent ability to provide oxygen species (i.e., oxidizing ability) for the efficient catalytic oxidative destruction of CVOCs.

Various types of catalytic materials have been studied for oxidative removal of CVOCs. Supported noble metal catalysts [12-15] show frequently more active and selective results than others, but they are generally expensive due to their scarcity, and poor structural stability is often observed with agglomeration of noble metal components under the heated atmosphere of reaction condition. Zeolites [16-19] have the advantage that their structure and acidity are easily adjustable with relatively cheap cost, but they also have several demerits of diversity of formed byproducts and vulnerability against coke deposition. Considering both aspects of cost and stability, transition metal based materials [20-32] are regarded as the prospective catalysts and numerous researches have been reported recently for the catalytic CVOCs removal (selected reports were summarized and compared in Table S1). In most cases, they are commonly used as composited form rather than being used as single phase in order to achieve more efficient catalytic process by modifying the characteristics of catalyst toward more appropriate degree in various aspect. For the supported catalytic materials, Al-based materials are most frequently used as the supporting material [12-15,32-35]. They can contribute to the heterogeneous catalysis by

†To whom correspondence should be addressed.
E-mail: kimwb@postech.ac.kr

providing outstanding textural properties (adsorption sites) where the gas phase reactants can be adsorbed, even if the catalytic oxidative destruction activity of themselves is negligible. Especially in the case of these CVOCs removal, they can also assist the catalytic removal process by accelerating the initiation step of C-Cl bond cleavage with their acid sites [36]. Moreover, their physicochemical properties as the supporting materials or the catalytic activity of themselves can be improved by forming mixed oxide with other elements [20,24-26]. Furthermore, the redox properties can be also enhanced by incorporation of additional active materials with strong oxidizing ability over these kinds of supporting materials [12-15, 32-35]. Thus, we hypothesized that hybridization of a transition metal based active material with excellent redox property and the Al-based supporting materials with sufficient surface area and abundant acid sites would be a prospective designing strategy for the efficient catalytic material. Among the various transition metals, copper is chosen as the active element because its oxidation state can be easily changed even at the relatively low temperature range, meaning that they can exhibit good activity toward redox interaction at low temperature [32,37,38]. Besides, cupric chloride is used as the Cu species incorporating agent. There are two advantages to use $CuCl_2$ as the active material: (1) calcination process is not required to deposit active materials on the surface, and (2) the $CuCl_2$ is a chloride form; therefore, its chemical stability under Cl-containing atmosphere would not be deteriorated. Indeed, it was confirmed from the XPS analysis results that the chemical state of Cu was not transformed (well maintained) under the reaction condition, even if the temperature of synthetic process was lower than reaction temperature.

In this paper, a series of supported $CuCl_x$ catalysts were synthesized by a wet impregnation of the $CuCl_2$ over the various supporting materials which consist of Al-based oxide. Single oxide of AlO_x, mixed oxide of $Al_1Ti_1O_x$ (Al-Ti mixed material) and the Y zeolite (Al-Si mixed material) were used as the Al-base supporting materials. The resulting composite catalysts were investigated for catalytic oxidation of 1,2-dichloroethane (DCE) as representative CVOCs using a typical fixed-bed catalytic reactor system, but herein the reaction condition would be somewhat harsh compared with previously reported researches (Table S1). According to the constituent elements of the supporting materials, characteristics of catalysts appeared to be quite differentiated, and the relationship between the physicochemical properties and their catalytic performances was observed and discussed. In addition, ZSM-5 zeolites (Si-based material) was also investigated for comparison, but the single oxide of TiO_x was not considered because it has extremely small surface area that it could not function as a supporting material where the active materials can be dispersed. Among the studied catalysts, $CuCl_2/Al_1Ti_1O_x$ composite shows the highest catalytic performance, which could be attributed to several beneficial effects associated with proper textural property, abundant acid sites and sufficient oxidizing ability.

EXPERIMENTAL

1. Preparation of Catalysts

Aluminum oxide and aluminum-titanium mixed oxide (molar ratio of Al : Ti=1 : 1) were synthesized by a typical sol-gel method according to the following procedure reported in our previous work [7]. Total moles of metals in the synthesized oxides were fixed to 0.2 mol. Pre-mixed solvent solution was prepared using 4.88 mL of acetylacetone (Sigma Aldrich, ≥99%) and 181 mL of 2-propanol (Sigma Aldrich, 99.5%) and calculated amount of aluminum-tri-sec-butoxide (Sigma Aldrich, 97%) was added in the solution, and then vigorously stirred for 0.5 h. Titanium (IV) isopropoxide (Sigma Aldrich, 97%) was dissolved with continuous stirring for 0.5 h, followed by adding 7.87 mL of 0.5 M nitric acid. The mixture was heated at 80 °C with stirring for two days to form viscous gel and evaporate solvent, and resultants were calcined in air atmosphere at 600 °C for 5 h to obtain the Al-Ti oxides. For the $CuCl_2$ incorporation, four kinds of oxide materials (Y zeolite, ZSM-5 zeolite, aluminum single oxide and aluminum-titanium mixed oxide) were selected as the supporting material. Y zeolite (Alfa Aesar, 45868) and ZSM-5 zeolite (Acros Organic, 279571000) were purchased as commercial products, and they were calcined at 550 °C for 5 h before used. Deposition of $CuCl_2$ on the prepared supporting material was carried out using a wet impregnation method. Calculated amounts of $CuCl_2{\cdot}2H_2O$ (Sigma Aldrich, 221783) were dissolved in deionized water (DI). The precursor solutions were mixed with supporting materials and sonicated for 0.5 h to allow the active species to be well impregnated, then dried overnight at 120 °C to evaporate DI. Hereafter, each supporting material was denoted as @Y, @ZSM5, @Al and @AlTi, and the # wt% $CuCl_2$ supported catalysts were named as #'support name'. For comparison, unsupported $CuCl_2$ was prepared by simply drying $CuCl_2{\cdot}2H_2O$ overnight at 120 °C and denoted as bulk-$CuCl_2$.

2. Physicochemical Characterizations of Catalysts

X-ray diffraction (XRD) patterns of prepared catalysts were obtained on Ultima IV (Rigaku) using a Cu-Kα radiation source X-ray in the 2θ range of 10° to 80°. The N_2 adsorption-desorption isotherms were carried out using ASAP 2020 and ASAP 2010 equipment (Micromeritics), and Brunauer-Emmett-Teller (BET) method was used to calculate the specific surface area. Scanning electron microscopy (SEM) and energy dispersive X-ray spectrometry (EDS) were used to observe the morphological characteristics of the surface of prepared catalytic materials on S-4800 (HITACHI). The amount and strength of the acid site on the surface of prepared catalysts were investigated by ammonia temperature programmed desorption (NH_3-TPD). Before the NH_3-TPD measurement, the catalysts were pretreated at 300 °C for 1 h under He atmosphere to remove contaminants (such as moisture) on the surface of catalyst, then cooled to 90 °C and exposed to NH_3 gas for 1 h. To remove physisorbed NH_3 on the surface, the catalysts were purged at 90 °C for 0.5 h under He atmosphere. Purging with He gas flow, desorption of the chemisorbed NH_3 on the surface of catalysts was analyzed within the temperature range of 90-700 °C and the ramping rate was 10 °C min^{-1}. During the NH_3-TPD measurement, all of the heat and gas flow was controlled by BELCAT-II (MicrotracBEL) and the exhaust gas was analyzed by HPR-20 (Hiden Analytical) mass spectrometry. The kinds of acid sites were classified by the ammonia Fourier-transform infrared spectroscopy (NH_3-FTIR) using NICOLET iS50 (ThermoFisherScientific). The catalysts were pretreated at 300 °C for 0.5 h under He atmosphere, then cooled to 50 °C and exposed to NH_3 gas for 0.5 h. After the removal of phy-

sisorbed NH_3 on the catalyst surface by He purging for 0.5 h at 50 °C, the FT-IR spectra were obtained. H_2 temperature-programmed reduction (H_2-TPR) was performed on BELCAT-II (MicrotracBEL) equipment, to investigate reducibility of the catalysts. The catalysts were reduced under H_2 atmosphere within the temperature range of 90-800 °C at the ramping rate of 10 °C min^{-1}. The amount of consumed H_2 by the reduction was measured with a thermal conductivity detector (TCD). The composition and oxidation states of the catalyst surface elements were investigated from the XPS spectra, which were obtained on K-ALPHA+ (ThermoFisherScientific) equipment (All of the XPS data were calibrated based on C 1s spectra).

3. Measurement of Catalytic Performance

Catalytic oxidation reaction of DCE was performed on a typical fixed-bed flow reactor system (Fig. S1(a)). Liquid phase DCE was evaporated in a jacketed glass saturator with the temperature control system, and the generated DCE vapor was carried by a He flow. To make desired feed stream condition, O_2 flow and another He flow were mixed to the DCE vapor flow stream. The resultant gas mixture consisted of 20% O_2 and 1,150 ppmv DCE balanced with He, and the total flow rate was maintained at 100 ml min^{-1}. Catalytic performance was measured in the temperature range of 200 to 500 °C with 50 mg of each catalytic material, the gas hourly space velocity (GHSV) was fixed to 120,000 mL h^{-1} g_{cat}^{-1}. The temperature of fixed bed reactor system during the catalytic oxidation reaction was controlled in a 50 °C interval step mode (details in Fig. S1(b)), and the experimental data were measured five times for each temperature and their average values were used to represent the catalytic performance at that temperature. The stability test was also performed at 400 °C for 80 h with 50 mg of catalysts (1,050 ppmv DCE, 20% O_2 balanced with He and GHSV condition of 120,000 mL h^{-1} g_{cat}^{-1}). Reactant or product gas mixtures were analyzed by 7890A (Agilent) on-line gas chromatography system with flame ionization detector (FID) and thermal conductivity detector (TCD). Commercial reference gas mixtures were calibrated to estimate the concentrations of DCE, CO and CO_2. The concentrations of other compounds were calculated by converting GC peak area, based on the FID signals with relative response factors.

RESULTS AND DISCUSSION

1. Characterization of the Catalysts

Textural properties of prepared catalysts were investigated by N_2 adsorption-desorption isotherm with BET calculation (Fig. 1 and S2); the results are summarized in Table 1. Single component of $CuCl_2$ without support, i.e., bulk-$CuCl_2$, revealed very small specific surface area and total pore volume. Consequently, bulk-$CuCl_2$ exhibited negligible value of conversion compared with that of other catalytic materials tested in this work. On the other hand, supporting materials showed sufficiently high surface area and pore volumes larger than 250 m^2 g^{-1} and 0.2 cm^3 g^{-1}, respectively. Thus, it could be expected that introduction of the supporting materials with superior textural properties would be helpful to increase the accessibility of gas phase reactants. Although the surface area and pore volume frequently decreased as the amount of deposited $CuCl_2$ was increased on the surface, supported $CuCl_2$ catalytic materials still maintained high values of surface area and pore volumes larger than 200 m^2 g^{-1} and 0.15 cm^3 g^{-1}, leading to much higher conversion values than that of bulk-$CuCl_2$.

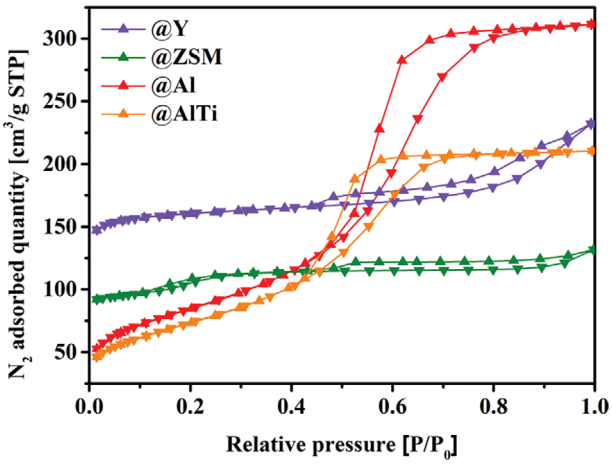

Fig. 1. N_2 adsorption-desorption isotherm profiles of supporting materials.

Table 1. Textural properties of prepared catalytic materials

Catalyst	S_{BET} [a] [m^2 g^{-1}]	V_{pore} [b] [cm^3 g^{-1}]
@Y	640.8	3.59×10^{-1}
2.5@Y	574.9	3.80×10^{-1}
10@Y	604.9	3.19×10^{-1}
@ZSM	395.5	2.09×10^{-1}
2.5@ZSM	331.0	1.96×10^{-1}
10@ZSM	322.5	1.58×10^{-1}
@Al	312.3	4.97×10^{-1}
2.5@Al	365.1	3.73×10^{-1}
10@Al	330.2	3.26×10^{-1}
@AlTi	266.7	3.26×10^{-1}
2.5@AlTi	259.4	3.04×10^{-1}
10@AlTi	212.9	2.42×10^{-1}
bulk-$CuCl_2$	2.283	8.04×10^{-3}

[a]Specific surface area calculated by BET method.
[b]Single point total pore volume (at P/P_0=0.995).

XRD patterns of the prepared catalytic materials were obtained (Fig. 2). Zeolites, @Y and @ZSM5 showed clear peaks of their own crystal structure and @Al had broad peaks of γ-Al_2O_3 phase with amorphous feature, whereas @AlTi did not possess any peak of specific crystal structure. When the mixed oxide is formed with similar molar ratio of metal elements, it has been reported that each species hindered the growth of crystalline phases; therefore, the crystal size could be too small to be detected over the resolution limit of XRD equipment [39,40]. In this respect, the nature of @AlTi with 1 : 1 molar ratio of Al to Ti would be similar accordingly. Meanwhile, all of the supported $CuCl_2$ catalysts did not reveal any peak related to cupric chloride phase. It could be possible that the deposited copper compounds exhibit amorphous feature when highly dispersed on the surface of support materials [41]. Thus, element mapping images of supported $CuCl_2$ catalysts were observed by

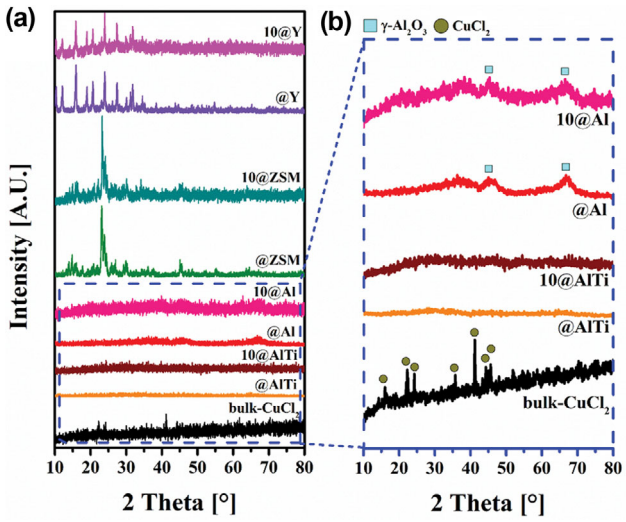

Fig. 2. XRD patterns of the prepared catalytic materials: (a) overall; (b) extended.

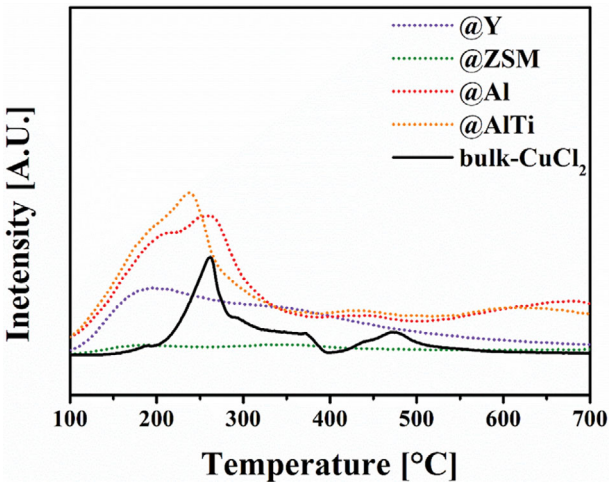

Fig. 3. NH_3-TPD profiles of the supporting materials and unsupported $CuCl_2$.

SEM-EDS (Fig. S3), because the XRD patterns in Fig. 2 could not provide any evidence for presence of $CuCl_2$ phase. It can be seen that Cu and Cl species obviously exist on the supporting material, and their high dispersion would be the reason for the undetectable peak.

The amounts of acid sites on the surface of prepared catalytic materials were estimated by NH_3-TPD measurement (Fig. 3 and S4). It is very important to identify the acidic properties of the surface of catalytic materials, because they play an important role of C-Cl bond cleavage causing dehydrochlorination process. In the case of supporting materials, zeolites exhibit lower amount of acid site compared with @Al or @AlTi; especially @ZSM show negligible acidity. Considering that the specific surface area of the zeolites is higher, the density of acid site is even much lower. It can be explained by chemical composition of each material (Table 2), that the specific atomic ratio of Si, Al and Ti elements is closely related to the number of surface acid sites. Al can produce not only Brønsted acid site when they are hydrated forming hydroxyl functional group [12], but also be converted to Lewis acid site by itself where the electron pair could be accepted [42]. On the other hand, Si has four valence electrons; therefore, it is very neutral in various chemical interactions including acid-base relation [43]. In this sense, @Al and @AlTi with numerous Al species have abundant acid sites, whereas @Y with small amount of Al have medium acidity, and @ZSM with Si-dominant composition [48] (Table 2 and Fig. S2) reveals negligible acidity (Fig. 3). Meanwhile, bulk-$CuCl_2$ also shows some acidity. The CuO_x, reported in our previous work [32] did not have its own acidity; thus the acidity of supported catalysts decreased as the content of incorporated CuO_x increased, but the $CuCl_2$ could be expected to have different effects when they are deposited. In fact, supported catalysts exhibited different acidic properties compared to their support, but interestingly they showed different tendencies depending on the supporting material (Fig. S4). Zeolite supported $CuCl_2$ catalysts revealed significantly increased amount of acid site according to the content of $CuCl_2$. Although their own acidity is poor, zeolites can provide very large surface for $CuCl_2$ deposition; then highly dispersed $CuCl_2$ with acidity could lead to dramatically increased number of surface acid sites. However, the others exhibited decreased number of acid sites, and it was somewhat recovered as the content of $CuCl_2$ increased, but showed still a small quantity compared to that of @Al or @AlTi. To understand the effect of $CuCl_2$ incorporation, NH_3-FTIR was performed (Fig. S5). Before the $CuCl_2$ was supported, Brønsted acid sites were dominant on the surface of @AlTi. Then, the intensity of Brønsted acid site was decreased to a certain degree as the $CuCl_2$ was deposited, and the signal of Lewis acid site was obviously increased. Thus, it seems that the number of total acid sites was decreased by the deposition of $CuCl_2$ that can occupy the Brønsted acid sites at the first, and then recovered some extent as the number of Lewis acid sites increased with more content of $CuCl_2$.

Table 2. Chemical composition of supporting materials

Catalyst	Atomic ration [%]					
	C[a]	O	Si	Al	Ti	Na
@Y	18.86	62.81	12.79	5.45	-	0.09
@ZSM	25.51	55.60	18.88	0.01	-	-
@AlTi	20.63	55.84	-	10.52	12.67	-

[a]Caused by carbon tape on the SEM sample holder

Reducibility properties of supporting materials were investigated by H_2-TPR, and the results are displayed in Fig. 4. When oxygen is the only element that can react with H_2, the reducibility (in terms of the amount of consumed H_2) can represent the ability to provide oxygen species, which is also directly associated with its oxidizing strength. Most of supporting materials show poor reducibility, except the @AlTi. Similar to the case of acidic properties, it could be also explained by the characteristics of constituent elements of each material (Table 2). Since Al and Si are typical elements, the oxidation state is rarely changed and thus there is scant amount of intrinsic defects (oxygen vacancy). On the other hand, since Ti is a transition metal which can possess various oxidation states (mainly Ti^{4+} and Ti^{3+}), it is much easier to generate oxygen vacancies in the

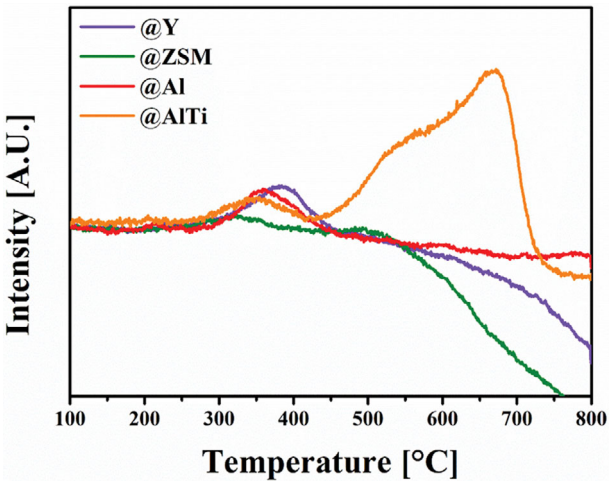

Fig. 4. H_2-TPR profiles of the supporting materials.

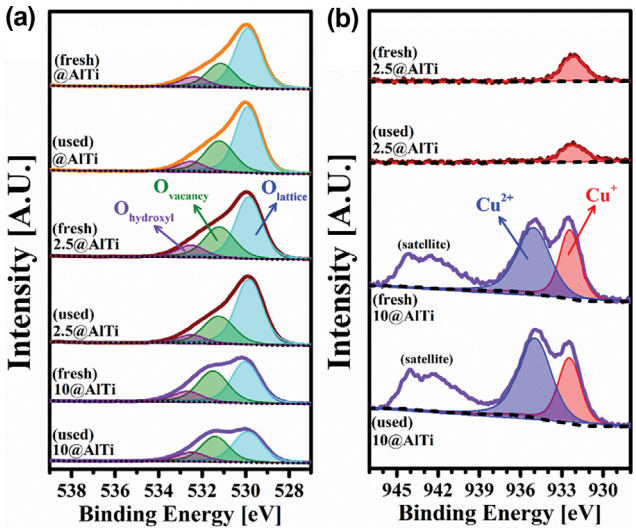

Fig. 5. XPS spectra of the fresh and used catalysts: (a) O 1s; (b) Cu 2p.

crystal structure. Moreover, extrinsic defects can be much more generated to maintain electroneutrality of the material when heteroatoms are doped into the Ti compounds. Such oxygen vacancies can facilitate the migration of oxygen atoms in the lattice, or can serve as sites where the dissociative adsorption of atmospheric O_2 can occur [44]. In this regard, the @AlTi, which is doped with Al heteroatom in Ti oxides, could reveal the highest reducibility among the supporting materials, and therefore it would be also expected that the @AlTi could well assist the oxidation process in catalysis. Indeed, @AlTi produced the largest amount of oxidation products (CO and CO_2) among the supporting materials (Fig. 6). However, $CuCl_2$-containing catalysts could not be analyzed unfortunately. Oxygen will also participate to the reaction with H_2, but in this case, Cl also reacts with H_2 to form HCl, making it practically impossible to separate each signal from the TCD detector. Thus, the influence of incorporated $CuCl_2$ at the oxidation process of catalysis should be investigated by XPS analysis along with the catalytic performance results.

Surface element composition and their chemical bonding environment were investigated by XPS analysis (Fig. 5 and summarized in Table 3). As displayed in Fig. 5(a), O 1s signal could be divided into three peaks of the oxygen species (1) contained in the surface hydroxyl group ($O_{hydroxyl}$), (2) attributed to adsorbed oxygen species on the vacancy site ($O_{vacancy}$), and (3) occupied at the lattice site ($O_{lattice}$) [45,46]. Among them, $O_{vacancy}$ is closely related with the oxidation process where the C-H bonds are broken by the surface adsorbed reactive oxygen species [11]. As the amount of incorporated $CuCl_2$ increased, the relative abundance of $O_{vacancy}$ also increased (Table 3); thus it could be expected that catalytic material with higher contents of $CuCl_2$ would possess higher activity for the oxidation process. Indeed, it is well associated with the catalytic oxidation results in which the catalytic materials with higher amount of $CuCl_2$ reveal higher yield for the completely oxidized products of CO_2 (Fig. S9(d)). Moreover, the relative abundance of $O_{vacancy}$ was decreased in 2.5@AlTi and 10@AlTi after used,; it also confirmed that the $O_{vacancy}$ sites play an important role in the catalysis. However, ironically, the relative abundance of $O_{vacancy}$ over the @AlTi increased after used. From the oxidized product profiles of CO and CO_2, it could be seen that the selectivity toward CO over the @AlTi was increased as the reaction temperature increased; thus, it seems that the oxygen species from the atmospheric oxygen molecule could not be transferred to CO well, but used to replenish the oxygen

Table 3. Surface chemical composition of fresh and used catalysts

Catalysts	Surface atomic ratio [%]									Relative abundance
	C	Al	Ti	$O_{hydroxyl}$	$O_{vacancy}$	$O_{lattice}$	Cu^{2+}	Cu^{+}	Cl	$O_{vacancy}/O_{lattice}$
@AlTi										
fresh	19.67	14.62	12.04	5.71	14.14	33.80	-	-	-	0.418
used	21.35	14.70	11.08	4.64	16.87	30.26	-	-	1.10	0.558
2.5@AlTi										
fresh	20.40	14.33	11.35	5.82	17.11	29.74	-	0.45	0.78	0.575
used	20.93	15.61	10.81	3.87	15.40	31.98	-	0.35	1.06	0.482
10@AlTi										
fresh	22.70	12.27	9.10	5.91	19.32	23.24	1.80	1.16	4.51	0.831
used	21.99	13.95	7.36	6.62	18.29	23.06	2.68	1.52	4.54	0.793

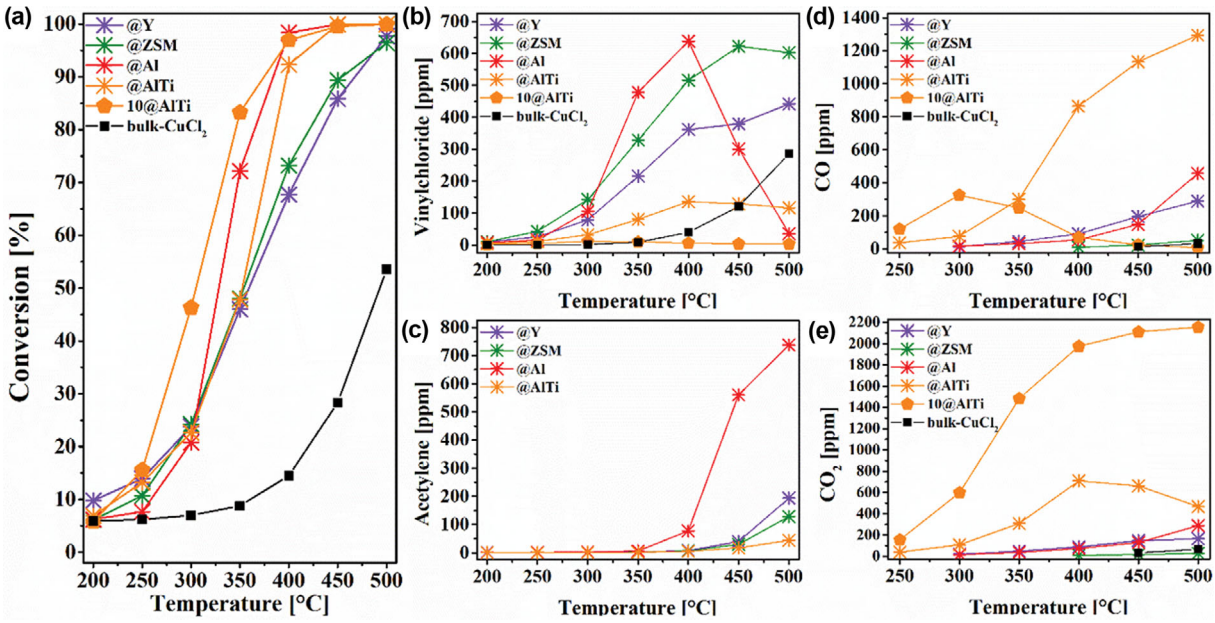

Fig. 6. Catalytic performance profiles with temperature changes for the catalytic oxidative destruction of DCE over the selected catalytic materials: (a) DCE conversion; (b) Vinyl chloride concentration; (c) Acetylene concentration; (d) CO concentration; (e) CO_2 concentration.

vacant site at the high reaction temperature. In the case of Cu species, there are different tendencies in 2.5@AlTi and 10@AlTi. Most of surface Cu species on 2.5@AlTi have the oxidation state of Cu^+, but the 10@AlTi possesses both oxidation states of Cu^{2+} and Cu^+ [47]. It seems that the increase of the relative abundance of $O_{vacancy}$ according to the $CuCl_2$ incorporation likely took place because the oxygen vacancy generated to maintain electroneutrality as the Cu^{2+} ion in the precursor became Cu^+ during the highly dispersed deposition process on the @AlTi surface. In addition, excess amount of Cu^{2+} after highly dispersed seems to be locally agglomerated, forming a cluster (Fig. S3) without change of the oxidation state of Cu^{2+}.

2. Catalytic DCE Decomposition Performance

The experimental results of catalytic oxidation of DCE were divided and displayed (Fig. 6 for supports and selected catalytic material, and Fig. S6 to S9 depending on the supporting material). The bulk-$CuCl_2$ exhibits quite low conversion at temperature below 450 °C; it would come from poor textural properties as previously mentioned. As the reaction temperature increases to 500 °C, the conversion value could reach 50%. However, it could be seen that most of converted DCE transformed to vinyl chloride rather than CO or CO_2, indicating that the dehydrochlorination process was dominant in catalysis and it could rarely lead to following oxidation step. It seems that the bulk-$CuCl_2$ had activity for the dehydrochlorination step based on its own acidity; but without the supporting material, it could not function as a site where the atmospheric O_2 could be adsorbed and transferred to intermediates. In the case of supporting materials, all of them show much higher conversion values compared to bulk-$CuCl_2$, but the diversity of reaction products is quite different according to the physicochemical characteristics of each material. The conversion values of zeolites were not too low, but most of reaction product remained as vinyl chloride. As expected at the reducibility analysis, it seems to be due to the poor oxidizing power which can cause the following oxidation step after the dehydrochlorination, like the result of bulk-$CuCl_2$. However, there was an interesting discovery that the @ZSM showed higher activity for dehydrochlorination compared with @Y though the @ZSM revealed negligible acidity. Moreover, there was no significant difference between dehydrochlorination activity of @ZSM based catalysts (Fig. S7(a)) even the $CuCl_x$ provided some acid sites (Fig. S4(b)). From these results, the dehydrochlorination mechanism over the @ZSM base catalysts could be assumed somewhat different with other catalytic materials using acid sites; this phenomenon should also be further investigated as another research topic in order to fully understand the dehydrochlorination mechanism. Since the @Al also had low reducibility, it could not lead most of converted DCE to be oxidized in the same manner. However, @Al revealed somewhat different results for the dehydrochlorination process compared to zeolites. Most of vinyl chloride, dehydrochlorinated product of DCE, was further dehydrochlorinated on the @Al at the temperature above 400 °C forming acetylene, the secondary dehydrochlorinated product of DCE. It seems that @Al has more sufficient acidic properties, which is closely related to dehydrochlorination process, rather than @Y or @ZSM. It could be expected that the @AlTi also generated similar products via dehydrochlorination because it had equivalent degree of acidity, but the composition of the products over @AlTi was quite different from that of @Al in reality. Unlike the other supporting materials, @AlTi possesses considerable reducibility, which could be directly associated with oxidizing ability; thus the dehydrochlorinated intermediates could be oxidized to form CO and CO_2. However, it still had a limitation that the main final product, CO, was not completely oxidized form, although the oxidation process could progress on the @AlTi. In brief, each supporting material had its own limitations to remove DCE via catalytic combustion, and it was the reason

why incorporation of active material, which could modify physicochemical characteristics of the surface, was considered. In the case of supported $CuCl_2$ catalysts, all of them showed remarkably increased production of oxidation products of CO and CO_2 compared to each supporting material (Fig. S6 to S9). Moreover, the selectivity toward CO_2, completely oxidized product, was increased as the amount of deposited $CuCl_2$ was increased. Therefore, it could be deduced that the active material of $CuCl_2$ could provide oxidizing strength enough to oxidize the dehydrochlorinated intermediates of vinyl chloride or acetylene. However, the incorporation of active phase had not only caused a positive effect on all aspects. In some cases, too much deposition decreased overall destruction efficiency, covering surface or pore structure [32]. More serious problems could be found in Fig. S10; it was observed that some of $CuCl_2$ incorporated catalysts emitted a series of polychlorinated ethylene species, whose undesired byproducts were frequently more toxic than the original contaminant, DCE. From the distribution of byproducts according to reaction temperature, it could be derived that the dehydrochlorination product of vinyl chloride with double bond was chlorinated (via substitution process, not addition reaction) to form dichloroethylene species (both cis- and trans-), and such substitutional chlorination side reaction was accelerated and further occurred as the reaction temperature increased, resulting in generation of more chlorinated products of trichloroethylene and tetrachloroethylene. In the case of tetrachloroethylene, they generally show the highest amount of emission at 450 °C, then decrease from the temperature above 500 °C, meaning that these polychlorinated compounds are even more difficult to be decomposed than vinyl chloride or acetylene intermediates. In this wise, it could be confirmed again that a good catalysis should not only exhibit high conversion, but also minimize the formation of undesired byproducts. Noteworthily, unlike the other supporting materials, the selectivity toward the completely oxidized product of CO_2 (rather than CO) was significantly high and the emission of polychlorinated byproduct was negligible, when the $CuCl_2$ was incorporated on @AlTi. Therefore, although the $CuCl_2$ could provide oxidizing power to oxidize vinyl chloride or acetylene, it was not enough to oxidize polychlorinated ethylene intermediates by itself alone, and it seems that only the @AlTi with reasonable reducibility could assist oxidative function of the copper-induced active site. In addition, the stability test for selected catalysts was also performed (Fig. S11). There were some decreases in catalytic performance during the stability test under harsh reaction condition, which seems to be caused by accumulative coke deposition on active sites. In the case of 10@Y, it shows a steady decrease in its catalytic activity, especially for oxidation process that the CO_2 yield has decreased by less than half of its initial value. On the other hand, all of the @AlTi based catalysts well maintained catalytic performance more than 80% degree of the initial performance even though the time on stream passed over 90 hours. Thus, it is expected that the higher oxidizing ability provides more resistance to coke deposition. Interestingly, there was almost no change in the distribution of the chemical state of copper species between the fresh and used catalysts (Fig. 5(b)), even if the temperature of synthetic process was lower than reaction temperature. Based on aforementioned investigations, we deduced that the physicochemical properties of catalytic materials should be well harmonized (such as textural properties, acidity, and reducibility) in order to achieve appropriate removal of CVOCs in terms of both destruction activity and product selectivity.

CONCLUSIONS

Catalytic destruction reaction of DCE was investigated over the $CuCl_2$ catalysts with various supporting materials. Based on the results in this work, it can be derived how each physicochemical characteristic would function on catalysis. Among the tested catalytic materials, $Al_1Ti_1O_x$ supported $CuCl_2$ catalysts showed most excellent catalysis in regard of high conversion with least formation of undesired byproducts. It could be achieved due to the harmony of (1) sufficient surface area where the gas phase reactants could well approach and be adsorbed, (2) abundant acid sites for dehydrochlorination, which could make the destruction of DCE to be initiated readily, and (3) excellent oxidizing ability, which could be originated by $CuCl_2$ and assisted by $Al_1Ti_1O_x$. The role of each physicochemical property in this catalysis and the designing strategy for composite catalytic materials discovered in this study would be able to contribute to the development of efficient catalyst based on non-precious materials for the sustainable CVOCs decomposition.

ACKNOWLEDGEMENTS

This research was supported by Basic Science Research Program through the National Research Foundation of Korea (NRF) funded by the Ministry of Science and ICT (NRF-2019R1A2C2088174), the Korea Institute of Energy Technology Evaluation and Planning (KETEP) and the Ministry of Trade, Industry & Energy (MOTIE) of the Republic of Korea (20212010100040) and the National Research Foundation of Korea (NRF) grant funded by the Korea government (MSIT) (NRF2021R1A5A1084921).

DECLARATION OF INTEREST STATEMENT

The authors declare that they have no known competing financial interests or personal relationships that could have appeared to influence the work reported in this paper.

SUPPORTING INFORMATION

Additional information as noted in the text. This information is available via the Internet at http://www.springer.com/chemistry/journal/11814.

REFERENCES

1. X. Zhang, Z. Xue, H. Li, L. Yan, Y. Yang, Y. Wang, J. Duan, L. Li, F. Chai, M. Cheng and W. Zhang, *J. Environ. Sci.*, **55**, 69 (2017).
2. P. Yang, M. Song, D. Kim, S. P. Jung and Y. Hwang, *Korean J. Chem. Eng.*, **36**, 1806 (2019).
3. J. W. Jeon, D. H. Lee, Y. S. Won and M. G. Lee, *Korean J. Chem. Eng.*, **35**, 744 (2018).
4. C. A. Santos, N. H. Phuong, M. J. Park, S. B. Kim and Y. M. Jo, *Korean J. Chem. Eng.*, **37**, 120 (2020).

5. C. Dai, Y. Zhou, H. Peng, S. Huang, P. Qin, J. Zhang, Y. Yang, L. Luo and X. Zhang, *J. Ind. Eng. Chem.*, **62**, 106 (2018).
6. S. Ojala, S. Pitkäaho, T. Laitinen, N. Niskala Koivikko, R. Brahmi, J. Gaálová, L. Matejova, A. Kucherov, S. Päivärinta, C. Hirschmann, T. Nevanperä, M. Riihimäki, M. Pirilä and R. L. Keiski, *Top. Catal.*, **54**, 1224 (2011).
7. S. Lee, H. Han, W. Yoon and W. B. Kim, *Appl. Catal. A Gen.*, **611**, 117970 (2021).
8. Q. Dai, S. Bai, H. Li, W. Liu, X. Wang and G. Lu, *Appl. Catal. B Environ.*, **168-169**, 141 (2015).
9. S. Cao, H. Wang, F. Yu, M. Shi, S. Chen, X. Weng, Y. Liu and Z. Wu, *J. Colloid Interface Sci.*, **463**, 233 (2016).
10. Y. Deng, S. Peng, H. Liu, S. Li and Y. Chen, *Front. Environ. Sci. Eng.*, **13**, 21 (2019).
11. H. A. Miran, M. Altarawneh, Z. T. Jiang, H. Oskierski, M. Almatarneh and B. Z. Dlugogorski, *Catal. Sci. Technol.*, **7**, 3902 (2017).
12. I. Maupin, L. Pinard, J. Mijoin and P. Magnoux, *J. Catal.*, **291**, 104 (2012).
13. L. Wang, M. Sakurai and H. Kameyama, *J. Hazard. Mater.*, **154**, 390 (2008).
14. A. Aranzabal, J. A. González-Marcos, J. L. Ayastuy and J. R. González-Velasco, *Chem. Eng. Sci.*, **61**, 3564 (2006).
15. Y. Gu, X. Jiang, W. Sun, S. Bai, Q. Dai and X. Wang, *ACS Omega*, **3**, 8460 (2018).
16. R. López-Fonseca, J. I. Gutiérrez-Ortiz, M. A. Gutiérrez-Ortiz and J. R. González-Velasco, *J. Catal.*, **209**, 145 (2002).
17. A. Aranzabal, J. A. González-Marcos, M. Romero-Sáez, J. R. González-Velasco, M. Guillemot and P. Magnoux, *Appl. Catal. B Environ.*, **88**, 533 (2009).
18. Q. Huang, X. Xue and R. Zhou, *J. Hazard. Mater.*, **183**, 694 (2010).
19. R. López-Fonseca, S. Cibrián, J. I. Gutiérrez-Ortiz, M. A. Gutiérrez-Ortiz and J. R. González-Velasco, *AIChE J.*, **49**, 496 (2003).
20. P. Yang, S. Fan, Z. Chen, G. Bao, S. Zuo and C. Qi, *Appl. Catal. B Environ.*, **239**, 114 (2018).
21. Z. Fei, C. Cheng, H. Chen, L. Li, Y. Yang, Q. Liu, X. Chen, Z. Zhang, J. Tang, M. Cui and X. Qiao, *Chem. Eng. J.*, **370**, 916 (2019).
22. P. Yang, S. Zuo, Z. Shi, F. Tao and R. Zhou, *Appl. Catal. B Environ.*, **191**, 53 (2016).
23. J. Mao, F. Tao, Z. Zhang and R. Zhou, *Environ. Sci. Pollut. Res.*, **25**, 27413 (2018).
24. S. Bai, B. Shi, W. Deng, Q. Dai and X. Wang, *RSC Adv.*, **5**, 48916 (2015).
25. A. Khaleel and M. Nawaz, *J. Environ. Sci.*, **29**, 199 (2015).
26. W. Yoon, S. Lee, Y. Noh, S. Park, Y. Kim, H. Ju Kim, H. J. Chae and W. Bae Kim, *ChemCatChem*, **12**, 5098 (2020).
27. P. Yang, Z. Shi, F. Tao, S. Yang and R. Zhou, *Chem. Eng. Sci.*, **134**, 340 (2015).
28. M. Tian, M. Ma, B. Xu, C. Chen, C. He, Z. Hao and R. Albilali, *Catal. Sci. Technol.*, **8**, 4503 (2018).
29. M. Tian, X. Guo, R. Dong, Z. Guo, J. Shi, Y. Yu, M. Cheng, R. Albilali and C. He, *Appl. Catal. B Environ.*, **259**, 118018 (2019).
30. F. Tao, S. Yang, P. Yang, Z. Shi and R. Zhou, *J. Rare Earths*, **34**, 381 (2016).
31. J. Wan, P. Yang, X. Guo and R. Zhou, *Chinese J. Catal.*, **40**, 1100 (2019).
32. S. Lee, W. Yoon, J. Ji, H. Ahn and W. B. Kim, *J. Environ. Chem. Eng.*, **10**, 108325 (2022).
33. T. K. Tseng, L. Wang, C. T. Ho and H. Chu, *J. Hazard. Mater.*, **178**, 1035 (2010).
34. Z. El Assal, S. Ojala, M. Zbair, H. Echchtouki, T. Nevanperä, S. Pitkäaho, L. Pirault-Roy, M. Bensitel, R. Brahmi and R. L. Keiski, *J. Clean. Prod.*, **228**, 814 (2019).
35. Y. Gao, J. Xiao, J. Ye, X. Huo and Y. Shen, *Korean J. Chem. Eng.*, **37**, 54 (2020).
36. T. Wang, Q. Dai and F. Yan, *Korean J. Chem. Eng.*, **34**, 664 (2017).
37. Ratnawulan, A. Fauzi and S. H. AE, *AIP Conf. Proc.*, **1868**, 060009 (2017).
38. N. A. Raship, M. Z. Sahdan, F. Adriyanto, M. F. Nurfazliana and A. S. Bakri, *AIP Conf. Proc.*, **1788**, 030121 (2017).
39. J. I. Gutiérrez-Ortiz, B. de Rivas, R. López-Fonseca, S. Martín and J. R. González-Velasco, *Chemosphere*, **68**, 1004 (2007).
40. W. Hua, C. Zhang, Y. Guo, G. Chai, C. Wang, Y. Guo, L. Wang, Y. Wang and W. Zhan, *Appl. Catal. B Environ.*, **255**, 117748 (2019).
41. M. S. Han, B. G. Lee, B. S. Ahn, D. J. Moon and S. I. Hong, *Appl. Surf. Sci.*, **211**, 76 (2003).
42. Y. N. Pushkar, A. Sinitsky, O. O. Parenago, A. N. Kharlanov and E. V. Lunina, *Appl. Surf. Sci.*, **167**, 69 (2000).
43. J. Pan and M. V. Ramakrishna, *Phys. Rev. B*, **50**, 15431 (1994).
44. M. Ramos, C. Díaz, A. E. Martínez, H. F. Busnengo and F. Martín, *Phys. Chem. Chem. Phys.*, **19**, 10217 (2017).
45. M. M. Can, S. Ismat Shah, M. F. Doty, C. R. Haughn and T. Frat, *J. Phys. D: Appl. Phys.*, **45**, 195104 (2012).
46. S. Jain, J. Shah, N. S. Negi, C. Sharma and R. K. Kotnala, *Int. J. Energy Res.*, **43**, 4743 (2019).
47. M. C. Biesinger, *Surf. Interface Anal.*, **49**, 1325 (2017).
48. A. Sápi, U. Kashaboina, K. B. Ábrahámné, J. F. Gómez-Pérez, I. Szenti, G. Halasi, K. János, N. Balázs, V. Tamásm, K. Ákosm and Z. Kónya, *Front. Mater.*, **6**, 127 (2019).

Supporting Information

Enhanced catalytic complete oxidation of 1,2-dichloroethane to CO_2 over the Al-based oxide supported $CuCl_x$ composite catalysts

Seungjun Lee, Wongeun Yoon, Iljun Chung, Junil Choi, Yongju Yun, and Won Bae Kim†

Department of Chemical Engineering, Pohang University of Science and Technology (POSTECH), 77 Cheongam-ro, Nam-gu, Pohang, Gyeongbuk 37673, Korea
(*Received 27 October 2022 • Revised 21 December 2022 • Accepted 31 January 2023*)

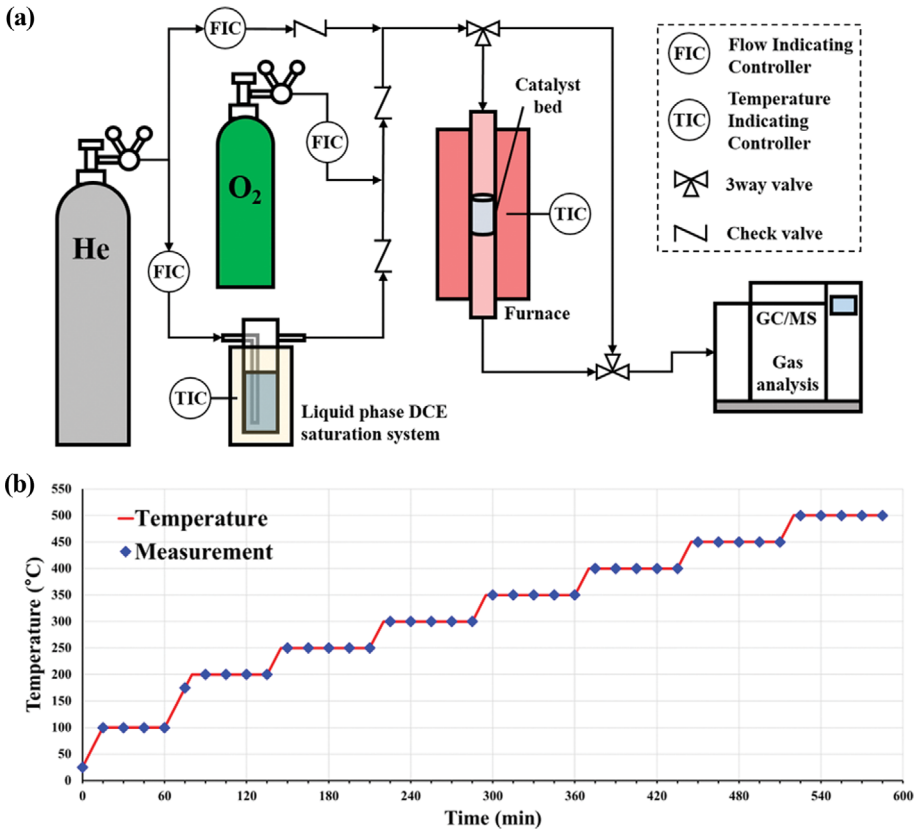

Fig. S1. Configuration of experimental system: (a) schema of fixed-bed flow reactor; (b) Temperature profile during the activity test.

During the single-run reaction operation, there was no dramatic differences between 4-5 times measurements (i.e., significant deactivation was not observed).

It could be indirectly found that the @ZSM used in present work would possess extremely high Si:Al ratio, by comparing N_2 adsorption-desorption isotherm profiles.

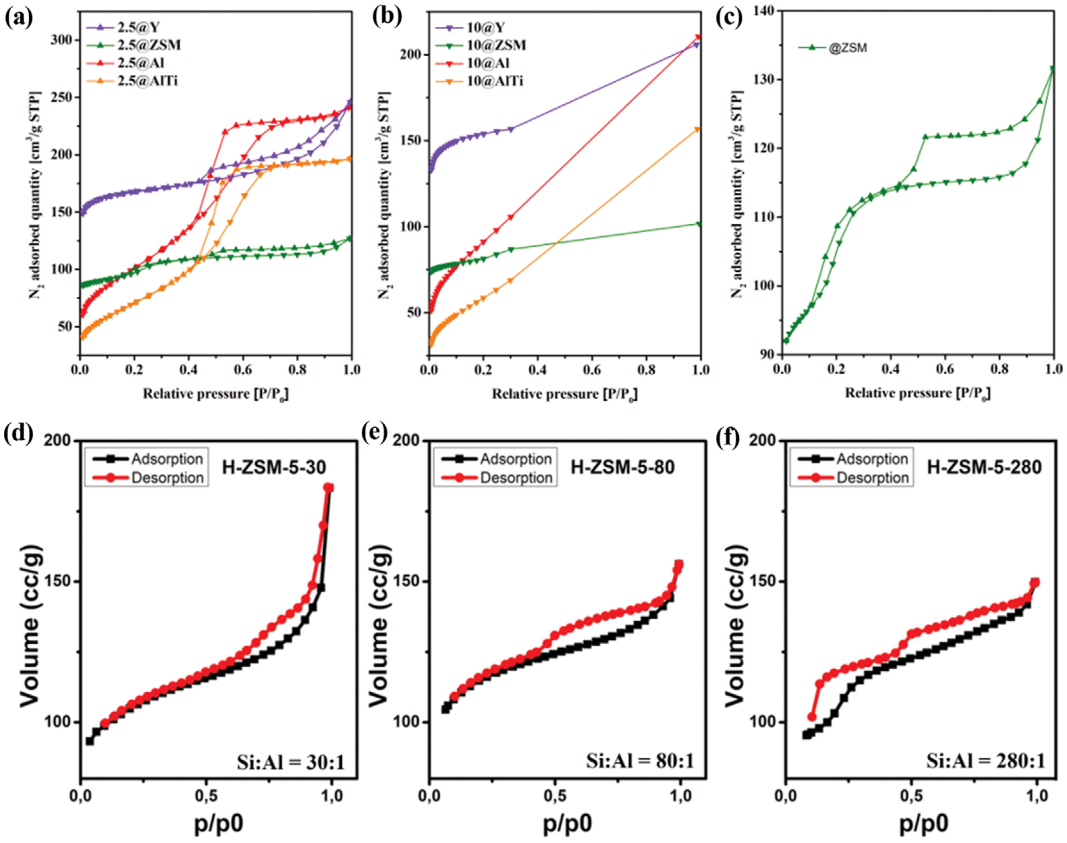

Fig. S2. N_2 adsorption-desorption profiles of (a): 2.5 wt% $CuCl_2$ incorporated catalysts; (b): 10 wt% $CuCl_2$ incorporated catalysts with selected P/P_0 range; (c): @ZSM with extended scale; (d), (e), (f): ZSM-5 with different Si:Al ratio by Sápi et al. (*Front. Mater. 6 (2019) 127*).

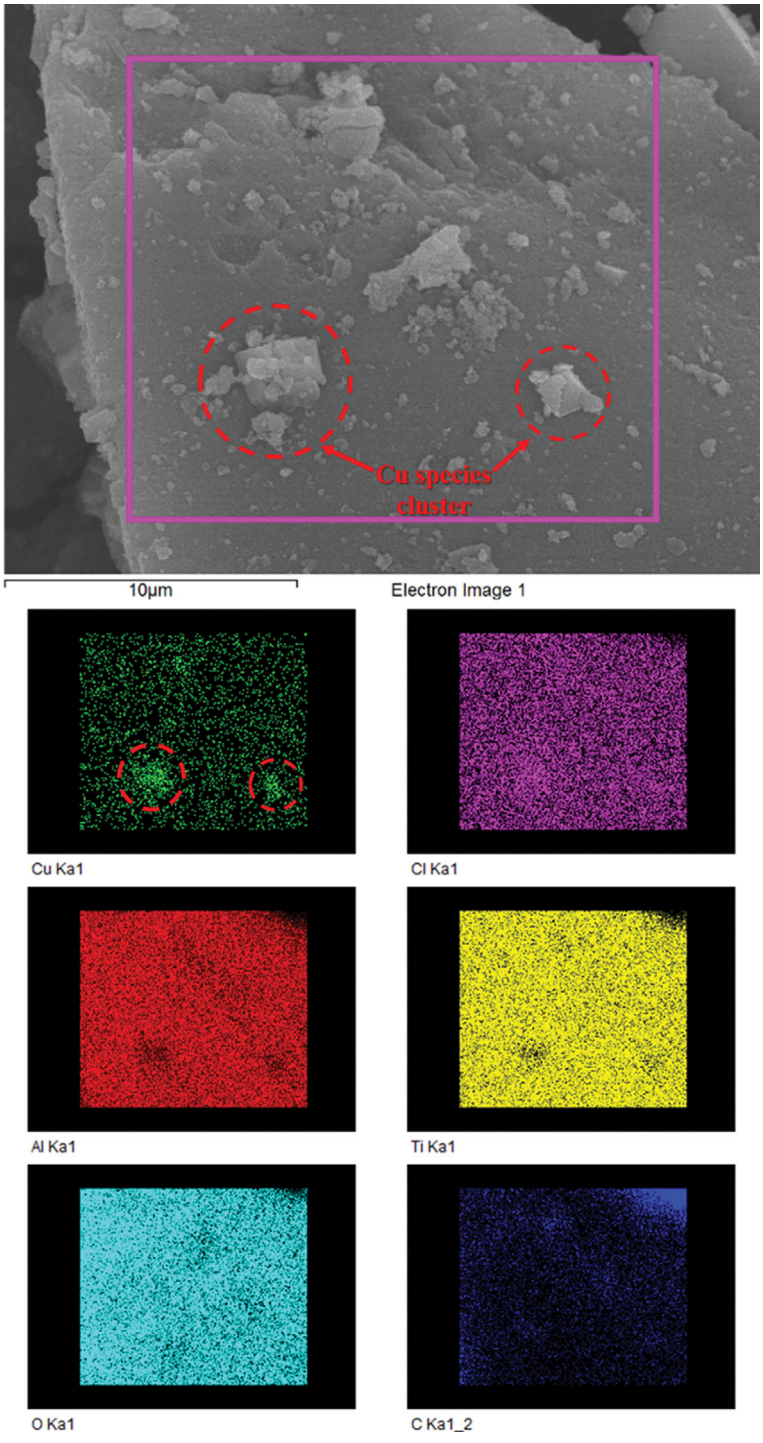

Fig. S3. Element mapping images of 10@AlTi catalyst.

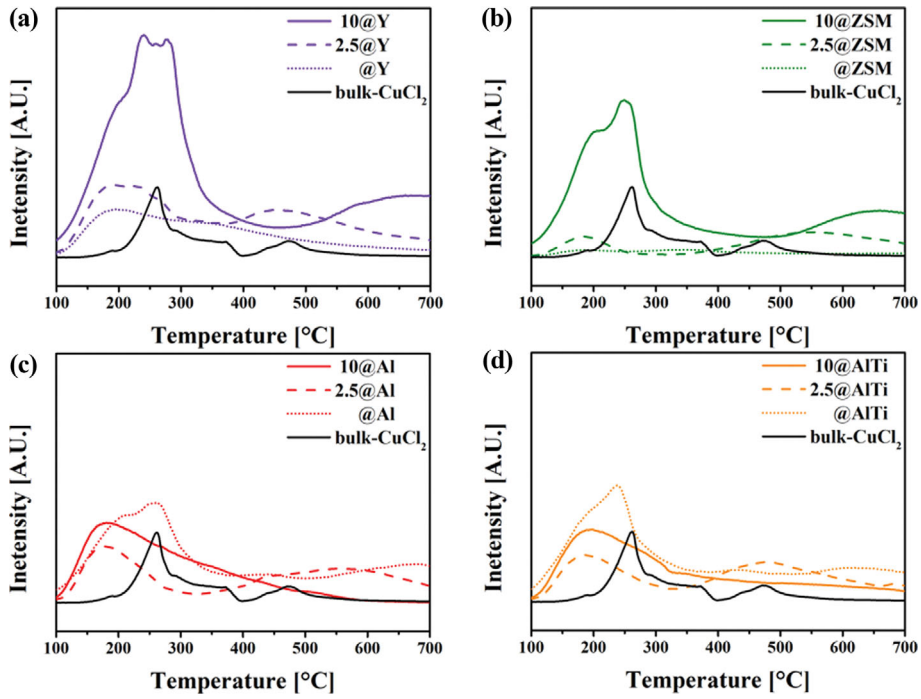

Fig. S4. NH_3-TPD profiles of supported $CuCl_2$ catalysts: (a) @Y supported; (b) @ZSM supported; (c) @Al supported; (d) @AlTi supported.

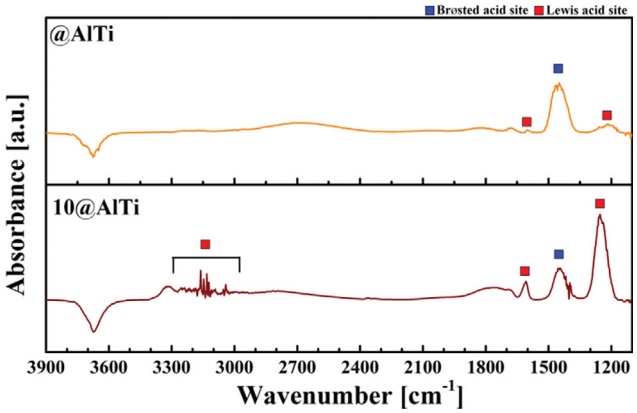

Fig. S5. NH_3-FTIR profiles of @AlTi and 10@AlTi.

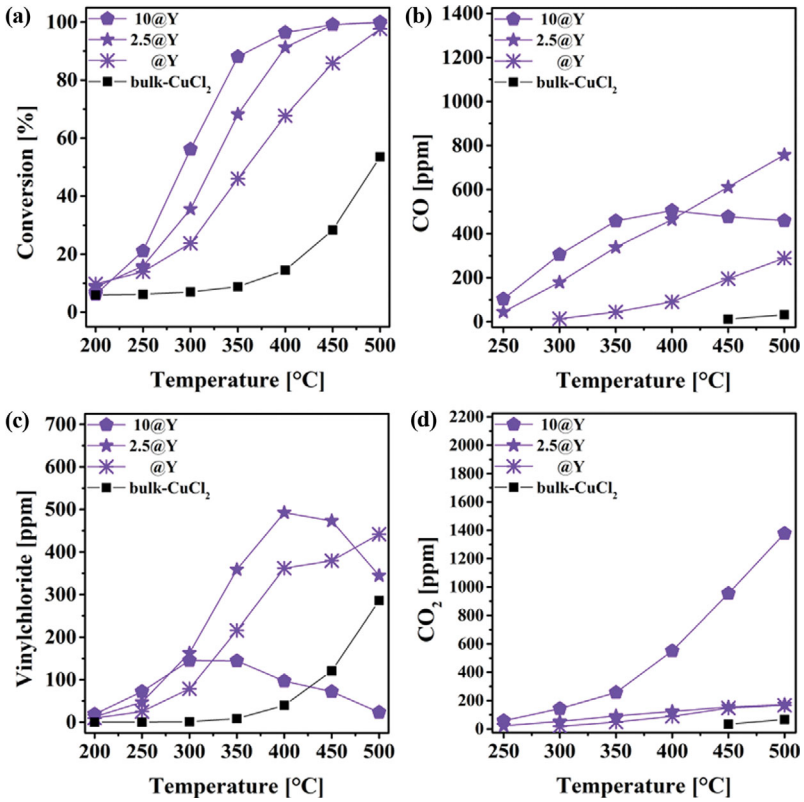

Fig. S6. Catalytic performance profiles of @Y supported $CuCl_2$ catalysts: (a) DCE conversion; (b) Vinylchloride concentration; (c) CO concentration; (d) CO_2 concentration.

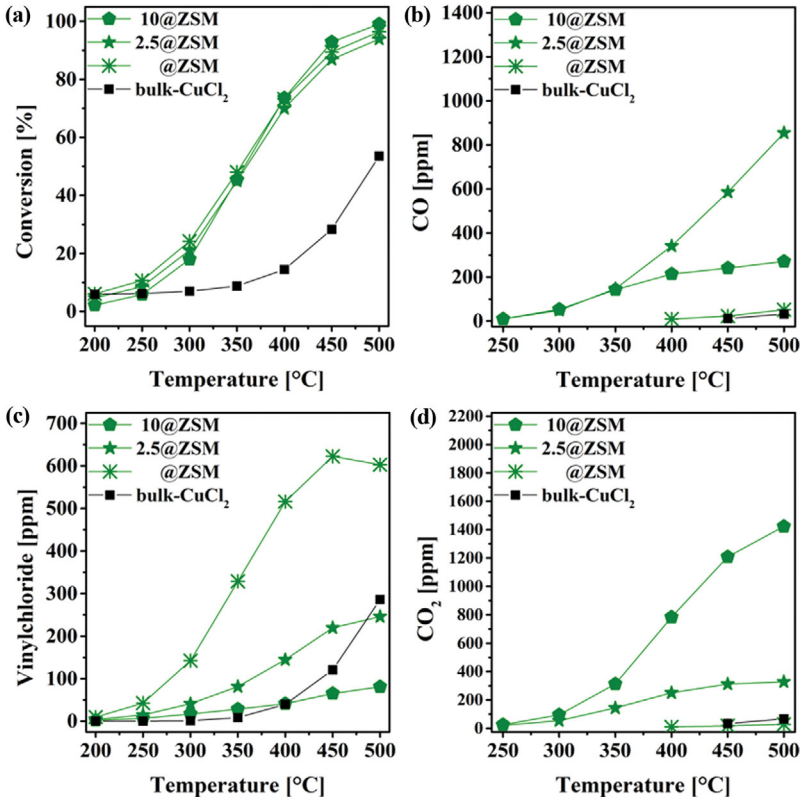

Fig. S7. Catalytic performance profiles of @ZSM supported $CuCl_2$ catalysts: (a) DCE conversion; (b) Vinylchloride concentration; (c) CO concentration; (d) CO_2 concentration.

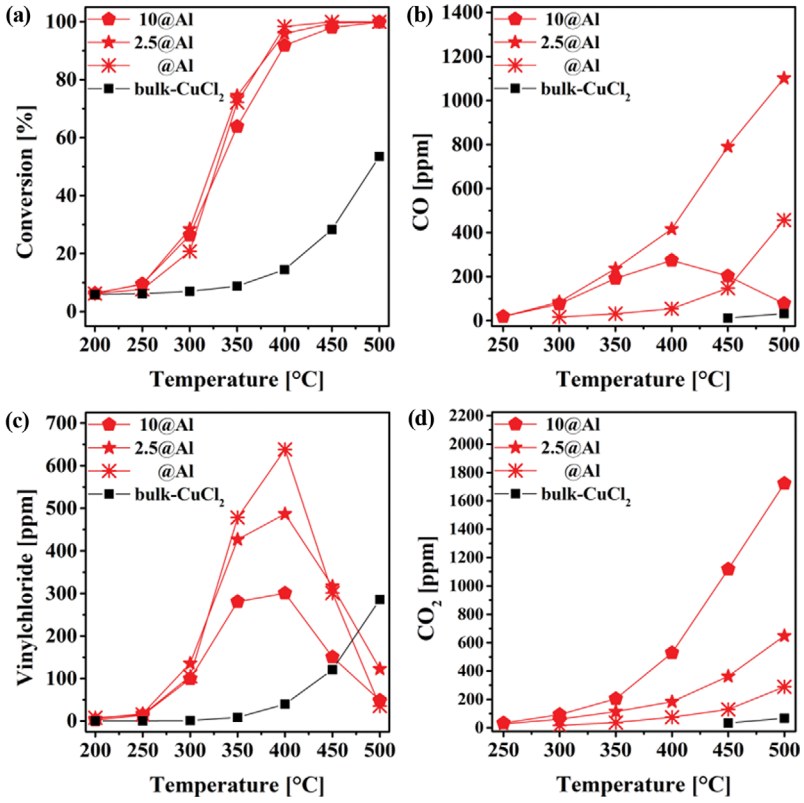

Fig. S8. Catalytic performance profiles of @Al supported $CuCl_2$ catalysts: (a) DCE conversion; (b) Vinylchloride concentration; (c) CO concentration; (d) CO_2 concentration.

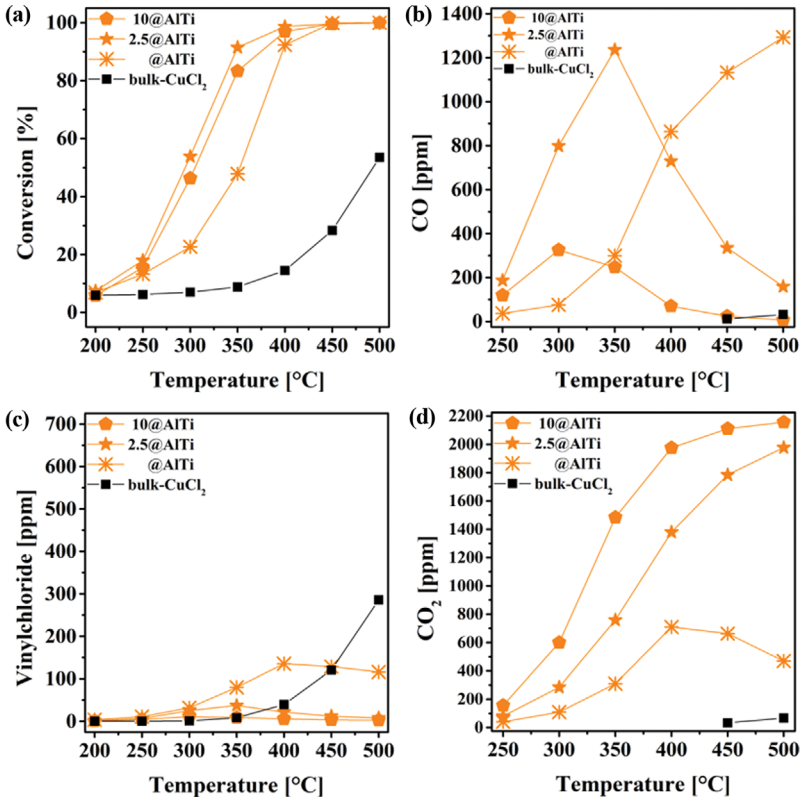

Fig. S9. Catalytic performance profiles of @AlTi supported $CuCl_2$ catalysts: (a) DCE conversion; (b) Vinylchloride concentration; (c) CO concentration; (d) CO_2 concentration.

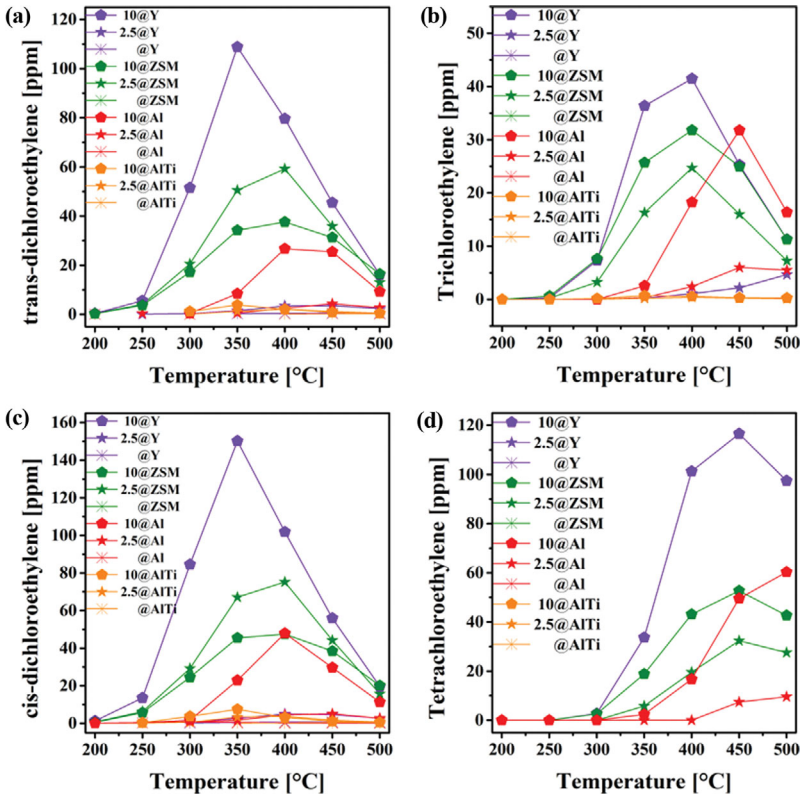

Fig. S10. Emission profiles of polychlorinated ethylene species over the supported $CuCl_2$ catalysts: (a) trans-dichloroethylene; (b) cis-dichloroethylene; (c) Trichloroethylene; (d) Tetrachloroethylene.

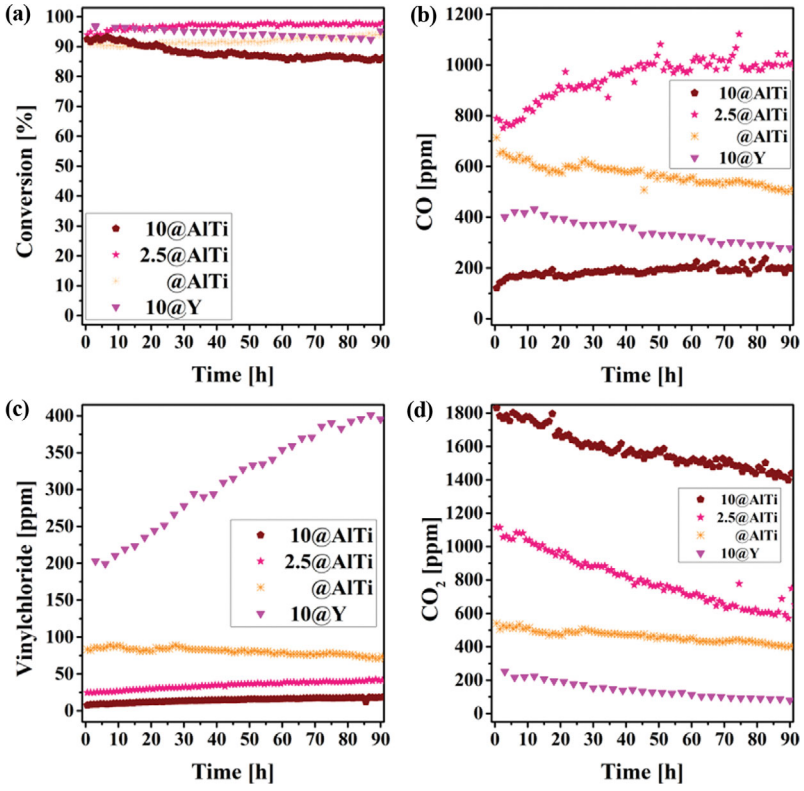

Fig. S11. Catalytic performance profiles at 400 °C with reaction times for the complete oxidation of DCE over the prepared catalytic materials: (a) Conversion; (b) Vinylchloride concentration; (c) CO concentration; (d) CO_2 concentration.

Table S1. Comparison table for previous reported researches and present work

Reference	Material	GHSV ($ml\ g_{cat}^{-1}\ h^{-1}$)	Reactant flow rate ($\mu mol\ g_{cat}^{-1}\ min^{-1}$)	Reaction rate ($\mu mol\ g_{cat}^{-1}\ min^{-1}$)		
				300 °C	350 °C	400 °C
Catal. Today. 375 (2021) 623-634	Cr/Ti	4,000	29.8	28.3		
RSC Adv. 5 (2015) 48916	Al-Ce	16,000	11.9	3.5	8.2	11.5
Environ. Sci. Pollut. Res. 25 (2018) 27413-27422	(Ce-Cr)/Nb	15,000	11.2	11.2		
Appl. Catal. B-Environ. 237 (2018) 114-124	Nb-W	9,000	6.7	6.0		
Appl. Catal. B-Environ. 259 (2019) 118018	Cr/(Mn-Co)	36,000	26.8	26.8		
J. Catal. 40 (2019) 1100-1108	Ce-Cr	9,000	6.7	6.7		
Chemosphere 68 (2007) 1004-1012	Mn-Zr	35,300	26.3	11.8	20.5	25.7
Appl. Catal. B-Environ. 222 (2018) 9-17	Co	35,300	26.3	18.4	24.9	
Appl. Catal. B-Environ. 191 (2016) 53-61	Ce-Cr	9,000	6.7	6.7		
J. Colloid Interface Sci. 426 (2014) 324-332	Mn-Ce-La	15,000	11.2	11.2		
Appl. Catal. A-General. 611 (2021) 117970	V/(Al-Ti)	60,000	44.6	19.8	32.6	41.3
J. Environ, Chem. Eng. 10 (2022) 108325	CuO_x/(Al-Ti)	60,000	51.3	33.4	47.6	50.9
Present work	**$CuCl_x$/(Al-Ti)**	**120,000**	**102.3**	**47.4**	**85.2**	**99.1**